Features of noncritical low-temperature and critical high-temperature anomalies of heat capacity in van der Waals $Cu(Ag)InP_2S(Se)_6$ crystals

V. Liubachko[1*], D. Szewczyk[2], V. Sokolenko[2], P. Gluchowski[2,3], K. Glukhov[1], A. Pogodin[1], V. Yevych[1], Yu. Vysochanskii[1]

1 Institute for Solid State Physics and Chemistry, Uzhhorod National University, 88000 Uzhhorod, Ukraine
2 Institute of Low Temperature and Structure Research, Polish Academy of Sciences, Okolna 2, 50-422 Wroclaw, Poland
3 Graphene Energy LTD, Curie-Skłodowskiej 55, 50-369 Wroclaw, Poland
**vitalii.liubachko@uzhnu.edu.ua*

Introduction

It has recently been established that the phenomenon of ferrielectricity in $CuInP_2S_6$ can be considered within the mixed Ising model with spins s = 1/2 and S = 1 [1]. These spins (or rather pseudospins) are associated with the ordering dynamics of Cu^+ cations in the double-well local potential and with the ordering/displacive dynamics of In^{3+} cations in the three-well local potential. Therefore, the occurrence of strong lattice anharmonicity is attributable to the presence of the indium sublattice, which manifests itself below 150 K. Conversely, at higher temperatures, the anharmonicity due to the copper sublattice activates the ionic conductivity and leads to the first order ferrielectric-paraelectric phase transition at $T_C \approx 315$ K, as well as to the existence of fluctuated polar clusters above T_C. The present study focuses on the temperature evolution of the heat capacity of $Cu(Ag)InP_2S(Se)_6$ crystals. The temperature range encompassed from 2 K to 370 K, thereby covering both the low-temperature region where quantum fluctuations play a pivotal role and the high-temperature region, where classical thermal fluctuations are predominant.

Experimental Results

For the study, $CuInP_2S_6$, $CuInP_2Se_6$, $AgInP_2S_6$ and $AgInP_2Se_6$ single crystals were grown using the Bridgman method.

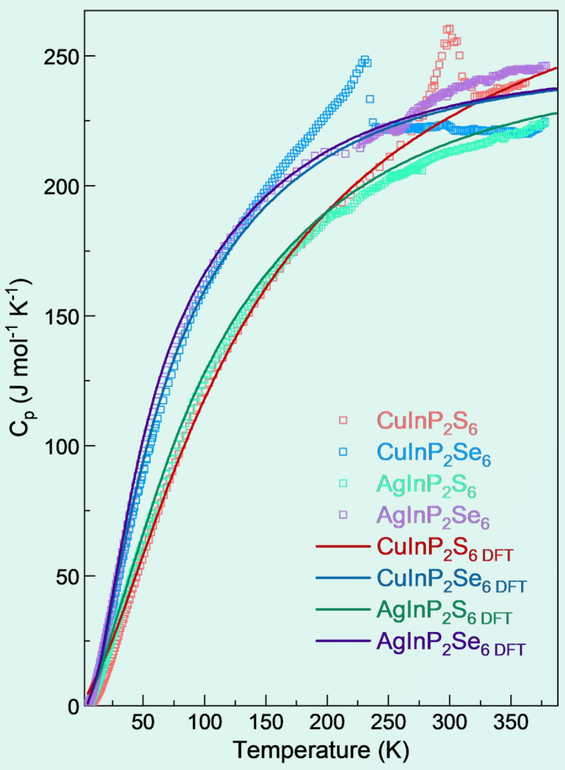

Figure 1. Experimental molar heat capacity (symbols) and DFT calculation (solid lines) of $CuInP_2S_6$, $CuInP_2Se_6$, $AgInP_2S_6$ and $AgInP_2Se_6$ crystals

As demonstrated in Fig. 1, the experimental measurements of the molar heat capacity of $CuInP_2S_6$ and $CuInP_2Se_6$ crystals confirm the presence of a phase transition at 304 K and 240 K, respectively, whereas no phase transition anomalies were observed in $AgInP_2S_6$ and $AgInP_2Se_6$ crystals.

The high-temperature critical C_p anomaly for a Bridgman-grown $CuInP_2S_6$ crystal was compared with the one of the crystal grown by the chemical transport reactions (CTR) method. As demonstrated in Fig. 2, the C_p anomaly of Bridgman-grown $CuInP_2S_6$ was more blurred in comparison to the compound obtained by the CTR method.

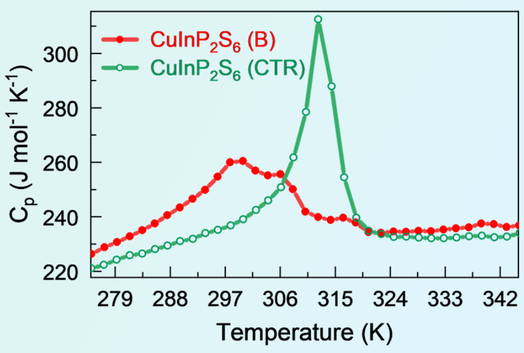

Figure 2. Phase transition in $CuInP_2S_6$, crystals grown by Bridgeman method (B) and chemical transport reactions (CTR)

Discussion

For all $CuInP_2S_6$, $CuInP_2Se_6$, $AgInP_2S_6$ and $AgInP_2Se_6$ crystals, a so-called "boson peak" was observed which is attributed to the specific nature of shear modes, which underlies the low-temperature heat capacity anomaly. $CuInP_2S(Se)_6$ compounds also show an anomalous increase in C_p/T^3 dependence upon cooling below the "boson peak". Such phenomenon is not observed in $AgInP_2S(Se)_6$ crystals. This anomaly may be classified as the appearance of a Schottky-like peak [2]. The existence of such an anomaly in $CuInP_2S(Se)_6$ is consistent with the mixed Ising model [3] and can be explained by fluctuations of S = 1 pseudospins that are related to the In^{3+} cations anharmonic dynamics in the three-well local potential. In particular, when silver replaces copper, in the centrosymmetric structure, the Ag^+ cations become firmly fixed at the center of the structural layer, thereby directly constraining the role of indium fluctuations at low temperatures. This assumption is corroborated by the temperature dependence of heat capacity calculated within the framework of the quantum anharmonic oscillator model [1]. The analysis indicated that the most significant increase in entropy within the ultralow-temperature region is linked to the anharmonic dynamics of indium. The model under consideration also predicts that the correlated relaxations related to Cu^+ cations s = 1/2 pseudospins can induce the ferroelectric clusters that occur above the transition from the ferrielectric to paraelectric state.

In order to extract the Schottky contribution to the $C_p(T)$ in $CuInP_2S(Se)_6$, a method similar to the approach employed in the study of magnetic compounds was used. In that method, an nonmagnetic the lattice C_p is taken as a reference and then subtracted from the curve of the magnetic sample [4]. As the reference the $C_p(T)$ of $AgInP_2S(Se)_6$ were used. In this study, the curves were normalized according to the following parameters: the temperature of the boson peak was set to 1, and the value of $C_p/T^3(T)$ at the boson temperature was set to 1. The results are shown in Fig. 3.

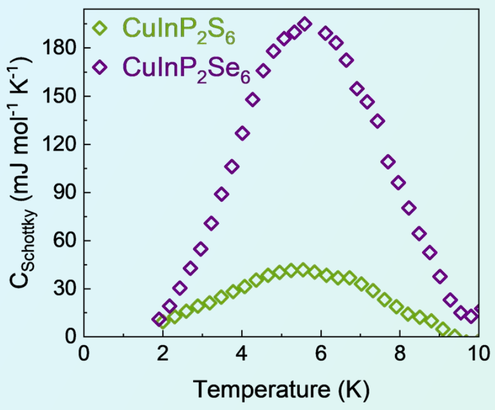

Figure 3. Extracted Schottky contribution to $C_p(T)$ in $CuInP_2S_6$ and $CuInP_2Se_6$ crystals

Conclusions

A comprehensive study of the heat capacity of $Cu(Ag)InP_2S(Se)_6$ crystals was conducted, enabling the estimation of the individual contributions to the heat capacity in these van der Waals materials.

References:
1. R. Yevych, V. Liubachko, V. Hryts, M. Medulych, A. Kohutych, Yu. Vysochanskii, Condens. Matter Phys. 27, 14701 (2024). https://doi.org/10.5488/cmp.27.14701.
2. V. F. Sears, Proc. Phys. Soc. 84, 951 (1964). https://doi.org/10.1088/0370-1328/84/6/314.
3. W. Selke, J. Oitmaa, J. Phys.: Condens. Matter 22, 076004 (2010). https://doi.org/10.1088/0953-8984/22/7/076004.
4. D. O'Flynn, M. R. Lees, and G. Balakrishnan. J. Phys.: Condens. Matter 26, 256002 (2014). http://dx.doi.org/10.1088/0953-8984/26/25/256002.

This work was supported by the Ministry of Education and Science of Ukraine (Grants: 0124U004302 – PH/41-2024; 0125U001555; 0126U001941) and HORIZONMSCA-2022-SE-01 (Grant 101131229 – Piezo2D).

Debye-Einstein Model

In order to describe the temperature dependence of the heat capacity, a combined Debye-Einstein model was used, which allows for the contribution of different types of crystal lattice vibrations. This approach is particularly relevant for complex solids, in which low-frequency acoustic phonons and high-frequency optical modes contribute differently to the total heat capacity. The molar heat capacity at constant volume was expressed as the sum of the Debye and Einstein contributions:

$$C_V(T) = n_D C_D(T) + \sum_{i=1}^{m} n_{E,i} C_{E,i}(T), \quad (1)$$

where n_D and $n_{E,I}$ is a number of vibrational modes, which satisfy the normalization condition $n_D + \sum_{i=1}^{m} n_{E,i} = 3N$, where N is a number of atoms in a formula unit. The Debye contribution is

$$C_D(T) = 9 n_D R \left(\frac{T}{\Theta_D}\right)^3 \int_0^{\Theta_D/T} \frac{x^4 e^x}{(e^x-1)^2} dx, \quad (2)$$

where R is gas constant, Θ_D is the Debye temperature. The Einstein contribution is

$$C_{E,i}(T) = 3 n_{E,i} R \frac{(\Theta_{E,i}/T)^2 e^{\Theta_{E,i}/T}}{\left(e^{\Theta_{E,i}/T}-1\right)^2}, \quad (3)$$

where $\Theta_{E,I}$ is the characteristic Einstein temperature of the correspondence optical mode.

Accordingly, the model enables the concurrent evaluation of a continuous spectrum of low-energy phonon excitations (the Debye model) and discrete local atomic vibrations (the Einstein model). The number of Einstein terms, m, was selected based on the complexity of the structure and the quality of the fit to the experimental data.

The parameters Θ_D, $\Theta_{E,i}$, as well as $n_{E,i}$, were determined by means of the least-squares method, with the aim of minimizing the deviation function: $\chi^2 = \sum_j [C_{exp}(T_j) - C_{calc}(Tj)]^2$, where $C_{exp}(T_j)$ are the experimental values of C_v at T_j, and $C_{calc}(T_j)$ are values, obtained from the model. To ensure an exact fit, the experimental C_p was converted to the C_v as $C_v = C_p - TV\frac{\alpha^2}{\beta}$, where V is the molar volume, α is the volume thermal expansion coefficient, β is the isothermal compressibility of the material.

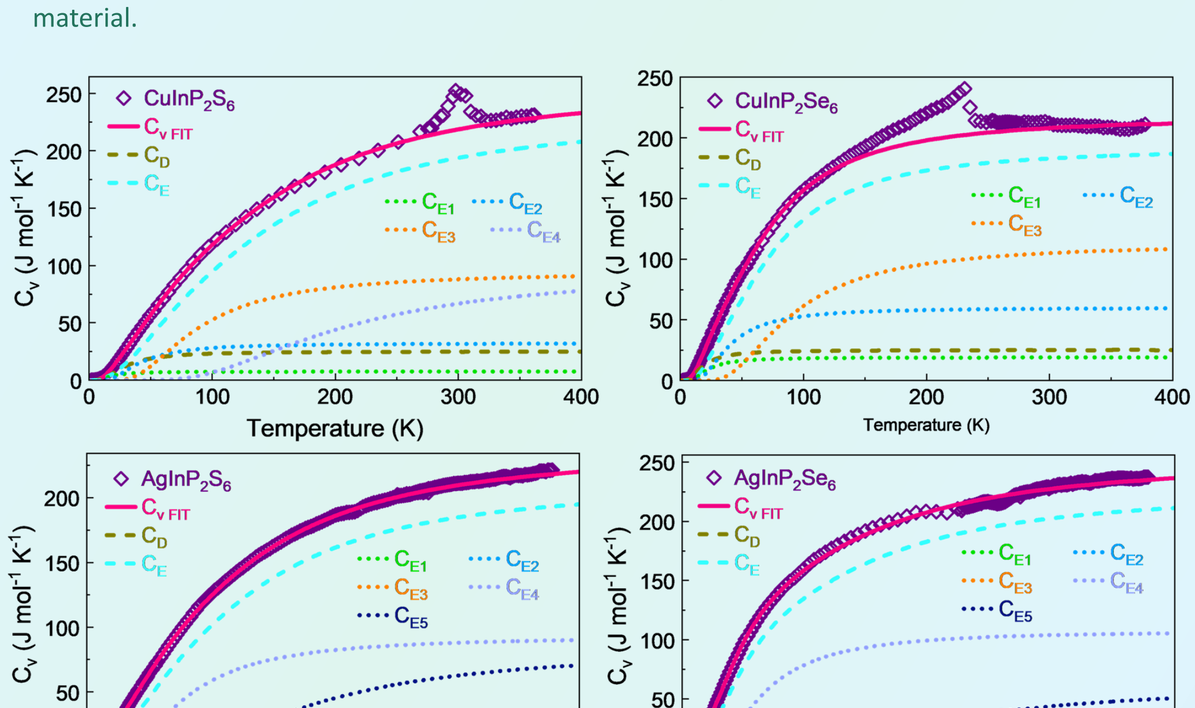

Figure 4. Results of fitting experimental C_v of $CuInP_2S_6$, $CuInP_2Se_6$, $AgInP_2S_6$ and $AgInP_2Se_6$ crystals. The Debye and Einstein contributions are shown

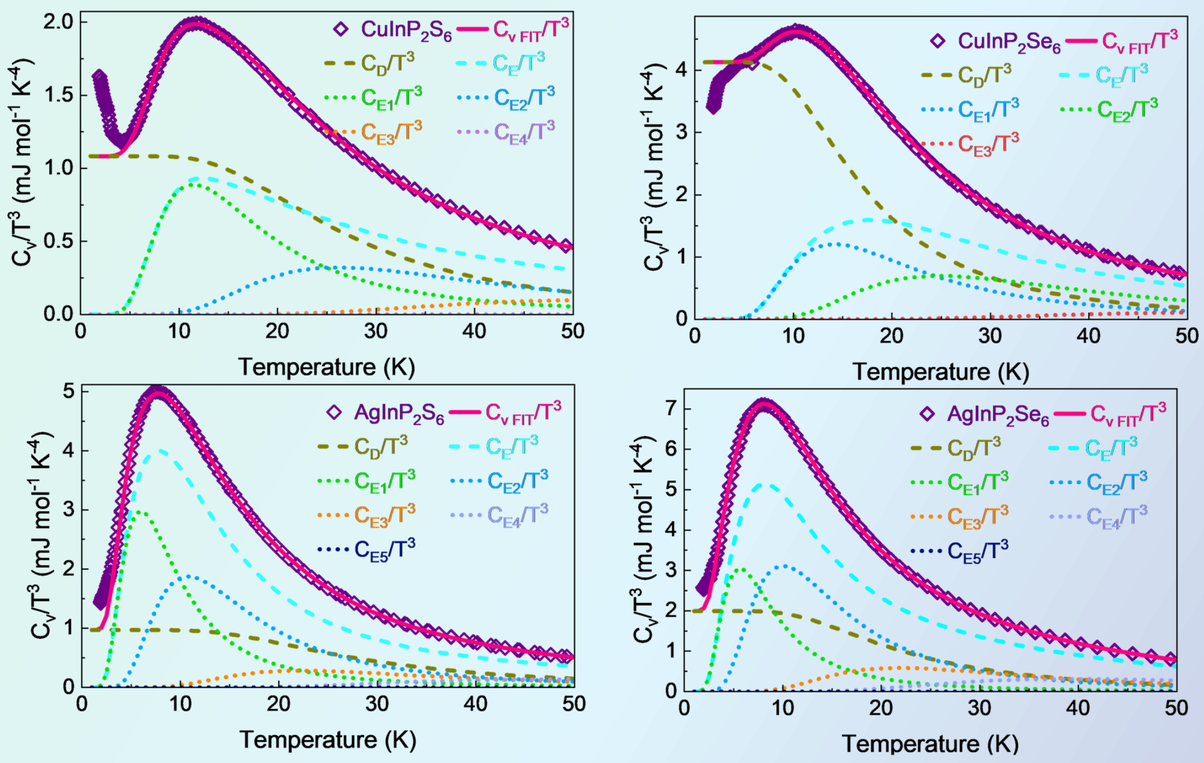

Figure 5. Results of fitting experimental C_v of $CuInP_2S_6$, $CuInP_2Se_6$, $AgInP_2S_6$ and $AgInP_2Se_6$ crystals in low temperature region in $C_v/T^3(T)$ scale. The Debye and Einstein contributions are shown